Phys. Status Solidi A **210**, No. 9, 1712–1718 (2013) / **DOI** 10.1002/pssa.201228771

physica status solidi a
www.pss-a.com
applications and materials science

# Reduced Coulomb interaction in organic solar cells by the introduction of inorganic high-*k* nanostructured materials

**Miriam Engel[1], David Schaefer[2], Daniel Erni[2], Niels Benson[*,1], and Roland Schmechel[1]**

[1] Institute for Nanostructures and Technology (NST), Faculty of Engineering, University of Duisburg-Essen and CENIDE – Center for Nanointegration Duisburg-Essen, 47057 Duisburg, Germany
[2] General and Theoretical Electrical Engineering (ATE), Faculty of Engineering, University of Duisburg-Essen and CENIDE – Center for Nanointegration Duisburg-Essen, 47057 Duisburg, Germany

Received 12 November 2012, revised 27 March 2013, accepted 27 March 2013
Published online 29 April 2013

**Keywords** Coulomb interaction, high-*k* materials, hybrid solar cells, nanostructures, organic solar cells

[*] Corresponding author: e-mail niels.benson@uni-due.de, Phone: +49 (0)203 379 1058, Fax: +49 (0)203 379 3268

In this paper a concept is introduced, which allows for reduced Coulomb interaction in organic solar cells and as such for enhanced power conversion efficiencies. The concept is based on the introduction of electrically insulating, nanostructured high-*k* materials into the organic matrix, which do not contribute to the charge transport; however, enhance the effective permittivity of the organic active layer and thereby reduce the Coulomb interaction. Using an analytical model, it is demonstrated that even at a distance of 20 nm to the organic/inorganic interface of the nanostructure, the Coulomb interaction in the organic semiconductor can be reduced by more than 15%. The concept is implemented using P3HT:PCBM solar cells with integrated high-*k* nanoparticles (strontium titanate). It could be demonstrated that in comparison to a reference cell without integrated nanoparticles, the power conversion efficiencies is improved by ~17%.



**1 Introduction** During the last decade an increase in the power conversion efficiency of organic photovoltaic cells up to almost 11% could be realized [1, 2]. This is mainly the result of developments in the device and material design, as well as optimized morphologies. Widely used is the bulk-heterojunction concept [3, 4] as well as tandem solar cell designs [5, 6]. However, one aspect which has received little attention during this development is the high Coulomb interaction in organic semiconductors, as the result of a low semiconductor permittivity ($\varepsilon_r \sim 3$–$4$) [7, 8]. This material property contributes to high exciton binding energies of up to 1.4 eV [9], reduces charge transport properties due to electrostatic interaction and leads to enhanced geminate pair formation [3, 10–12]. An enhancement of the material permittivity would reduce the influence of the Coulomb interaction and therefore have a beneficial effect on the maximum obtainable power conversion efficiency for organic solar cells. This can be achieved either by designing novel organic semiconductor materials with an enhanced permittivity [13], or by enhancing the effective permittivity of the organic active layer. The latter has been substantiated in a recent publication, by which we demonstrated facilitated exciton separation in pentacene on high-*k* substrates. This was ascribed to an effectively enhanced permittivity in the vicinity of the substrate/semiconductor interface and as such reduced electrostatic interaction between complementary charges [14]. In the current paper we demonstrate the feasibility of a concept to enhance the effective permittivity of organic solar cells, by the integration of electrically insulating, nanostructured high-*k* materials. The benefit of the organic/high-*k* interface for charge pair separation and the charge carrier transport is discussed using the charge carrier escape energy. Further, first P3HT:PCBM solar cells with integrated high-*k* strontium titanate ($SrTiO_3$) nanoparticles are realized, demonstrating a power conversion efficiency enhancement of ~17% in comparison to reference devices.

**2 Experimental** The solar cells were realized on commercially available OLED grade glass substrates covered with indium tin oxide (ITO). Poly(3,4-ethylenedioxythiophene) poly(styrenesulfonate) (PEDOT:PSS, Clevios P VPAl 4083) was deposited via spin coating and subsequently annealed for 10 min at 165 °C. All further processing was conducted in inert $N_2$ atmosphere. The active layer for both high-*k* and reference solar cells was prepared using a 1:0.78 blend of regioregular poly(3-hexylthiophene-2,5-diyl) (P3HT, Sepiolid P200, BASF) and [6,6]-phenyl-C61-butyric acid methyl ester (PCBM, Sigma–Aldrich) solved in chlorobenzene (10 mg $mL^{-1}$ P3HT). In order to be able to realize high-*k* organic solar cells, dried (150 °C under vacuum, 2 h) high-*k* strontium titanate ($SrTiO_3$, Iolitec) nanoparticles were added to a part of the reference solution, which has been stirred at 65–70 °C for 8 h in a concentration of 5 mg $mL^{-1}$. Further, ceramic grinding balls were added to the high-*k* solution for better dispersability of the $SrTiO_3$ nanoparticles. Both low-*k* dispersion and high-*k* dispersion were continuously stirred over night. Prior to the low-*k* solution/high-*k* dispersion deposition using a spin coater, both solution and dispersion were filtered. The low-*k* solution using a 0.7 μm filter, and the high-*k* dispersion using 2.7, 1.2, and 0.7 μm filters. Metal electrodes (50 nm calcium, 150 nm aluminum) were deposited by evaporation in high vacuum. In a final step the solar cells were annealed for 10 min at 140 °C. The active area of the solar cells is 20 $mm^2$.

The devices were characterized using a Keithley source-measure unit in the dark and under standard AM1.5 illumination. The current–voltage (*I–V*) characteristics were measured between −1 and +1 V under nitrogen atmosphere. Transmission measurements in a spectral range from 800 nm down to 300 nm were conducted using a Shimadzu UV-2550 UV–VIS spectrometer in combination with an integrating sphere. Here a glass/ITO/PEDOT:PSS layer stack was used as a reference. Further, the structure of the active layer was analyzed using a JEOL scanning electron microscope.

**3 Theoretical considerations** In order to quantify the influence of the organic/high-*k* material interface on the electrostatic charge carrier interaction in organic semiconductors, the following analytical model is used to describe the Coulomb interaction between complementary charges at the interface between low-*k* and high-*k* infinite large half-spaces.

The model considers a stationary charge $Q_s$ in a low-*k* material at a distance of 2.5 nm to a low-*k*/high-*k* interface, as well as a reference low-*k*/low-*k* interface. The model investigates the interaction of a test charge with the stationary charge. Further, image charges induced at the interface by the stationary and the test charge are considered. Both test and stationary charges carry a charge equal to $|Q| = nq$. Whereby $n$ is 1 and $q$ is the elementary charge.

The electrostatic interaction between the respective charges is described by the Coulomb interaction, with a force $F_{\mathrm{Coulomb}}$ of

$$F_{\mathrm{Coulomb}} = \frac{Q_s Q_t}{4\pi\varepsilon_0\varepsilon_r r^2}. \tag{1}$$

Here $r$ represents the distance between the charges, $\varepsilon_r$ the homogeneous, linear, material permittivity and $\varepsilon_0$ the vacuum permittivity.

The bound charge density induced by the charges $Q_s$ or $Q_t$, is described each as a single image charge $Q'$ as discussed by Jackson [15]. The equation used to approximate the image charge $Q'$ is given in the following:

$$Q' = \frac{\varepsilon_{r,\text{low-}k} - \varepsilon_{r,\text{high-}k}}{\varepsilon_{r,\text{low-}k} + \varepsilon_{r,\text{high-}k}} Q. \tag{2}$$

Equation (2) is valid for an interaction with the test charge in the low-*k* half space. The interaction scenarios considered here are illustrated in Fig. 1. Case A (Fig. 1a) represents the reference system with a low-*k*/low-*k* interface. Both half spaces are assigned a permittivity of 3. For case B (Fig. 1b) a low-*k*/high-*k* interface is considered. Here respective permittivities of 3 and 300 are taken into account for the low-*k*/high-*k* material. In consequence, only the Coulomb interaction between the stationary charge $Q_s$ and the test charge $Q_t$ needs to be considered for case A, while for case B also the interaction with the image charges $Q'_s$ and $Q'_t$ needs to be considered.

In order to analyze the total Coulomb force influencing the test charge, the concept of the escape energy $E_{\mathrm{escape}}$ is introduced. It describes the energy input needed to move $Q_t$ into infinity, away from the stationary charge as well as the higk-*k* interface, and can therefore be related to the difference in potential energy $\Delta E_{\mathrm{pot}}$ of the test charge at position $P_a$ and the reference point at $P_\infty$ at infinity:

$$E_{\mathrm{escape}} = -\Delta E_{\mathrm{pot}}. \tag{3}$$

The escape energy $E_{\mathrm{escape}}$ is calculated by integrating the effort to counteract the total Coulomb force $\boldsymbol{F}$ affecting the

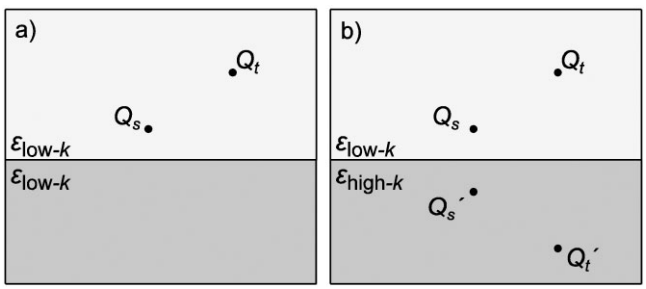


**Figure 1** (a) $Q_s$ and $Q_t$ above a low-*k*/low-*k* interface with a homogeneous permittivity of 3, (b) $Q_s$ and $Q_t$ above a low-*k*/high-*k* interface ($\varepsilon_{r,\text{low-}k} = 3/\varepsilon_{r,\text{high-}k} = 300$) with corresponding image charges $Q'_s$ and $Q'_t$.

test charge as shown in Eq. (4),

$$E_{\text{escape}} = -\int_{P_a}^{P_\infty} \boldsymbol{F}\cdot \mathrm{d}\boldsymbol{s} = -Q_t \int_{P_a}^{P_\infty} \boldsymbol{E}\cdot \mathrm{d}\boldsymbol{s} = Q_t[\varphi_{\text{total}}(P_\infty) - \varphi_{\text{total}}(P_a)] = -Q_t \cdot \varphi_{\text{total}}(P_a). \quad (4)$$

Here $\boldsymbol{E}$ describes the electric field. The electrical potential at $P_\infty$ is considered to be zero. It becomes evident that the escape energy $E_{\text{escape}}$ of the test charge can be calculated by the multiplication of the test charge $Q_t$ with the total electrical potential $\varphi_{\text{total}}$ at position $P_a$. The potential $\varphi_{\text{total}}$ is analytically calculated by a superposition of the potential of the stationary charge $Q_s$ as well as the image charges $Q'_s$ and $Q'_t$ ($\varphi_{\text{total}} = \varphi_s + Q'_s + Q'_t$). Here the specific potentials $\varphi_i$ are calculated as

$$\varphi_i = \frac{Q_i}{4\pi\varepsilon_0\varepsilon_r r}. \quad (5)$$

Here $r$ represents the absolute distance between the test and the stationary charge.

Please note that the presented formalism for the total potential $\varphi_{\text{total}}$ bears a minor subtlety owing to the simultaneous movement of the image charge $Q'_t$ during the "escape" of the test charge $Q_t$. Even though a direct contribution from $Q_t$ will alter the total potential $\varphi_{\text{total}}$ according to its changing position, and therefore a changing position of $Q'_t$, it is not relevant whether the image charge $Q'_t$ is doing work or not. Here, we are focusing on the escape process only, leaving aside the changing energy input (due to polarization) into the high-$k$ material.

The result of this escape energy evaluation is presented in the following for the cases A and B.

Illustrated in Fig. 2a is the escape energy of the test charge for case A. The radial escape energy dependence subject to the distance between test and stationary charge is the result of the homogeneous material permittivity of 3 at the low-$k$/low-$k$ interface. The escape energy distribution changes significantly for case B, where the low-$k$/high-$k$ interface ($\varepsilon_{r,\text{low-}k} = 3/\varepsilon_{r,\text{high-}k} = 300$) is considered. Here, the escape energy distribution is to a large degree dependent on the distance between the test charge and the stationary charge as well as the interface (Fig. 2b). The influence of the interface is a consequence of the interaction between the test charge $Q_t$ and the image charges $Q'_t$ and $Q'_s$.

The relative change of the escape energy between case A and B is quantified by Fig. 2c. The graph demonstrates that the benefit of a reduced escape energy due to the introduction of a high-$k$ interface increases, with an increase in the test charge/interface distance. At a distance of 20 nm to the stationary charge and perpendicular to the high-$k$ interface a reduction of the escape energy by 30% is found, while at a distance of 45 nm the escape energy is reduced by over 40%, for the used example.

For case B the reduced interaction between the stationary charge and the test charge can be ascribed to a screening of the stationary charge $Q_s$ by its image charge $Q'_s$. Here this screening results into an effective $Q_s$ of:

$$Q_{s,\text{effective}} = Q_s + Q'_s = \left(1 + \frac{\varepsilon_{r,\text{low-}k} - \varepsilon_{r,\text{high-}k}}{\varepsilon_{r,\text{low-}k} + \varepsilon_{r,\text{high-}k}}\right)\cdot Q_s \approx 0.02 \cdot Q_s. \quad (6)$$

While this screening effect may be beneficial for test charges at a distance to the high-$k$ interface beyond the red dashed 0% relative escape energy change line in Fig. 2c, an enhancement in the escape energy is found for test charges close to the high-$k$ interface due to image charge interaction. By considering Fig. 3, however, which illustrates the direction of the Coulomb force for case B, it becomes clear that due to the enhanced interaction of the test charge with the high-$k$ interface, the Coulomb force has a major component perpendicular to the interface. In consequence charge carrier transport in parallel to the high-$k$ interface does not require additional energy. In other words, charge carrier interaction close to the high-$k$ interface is

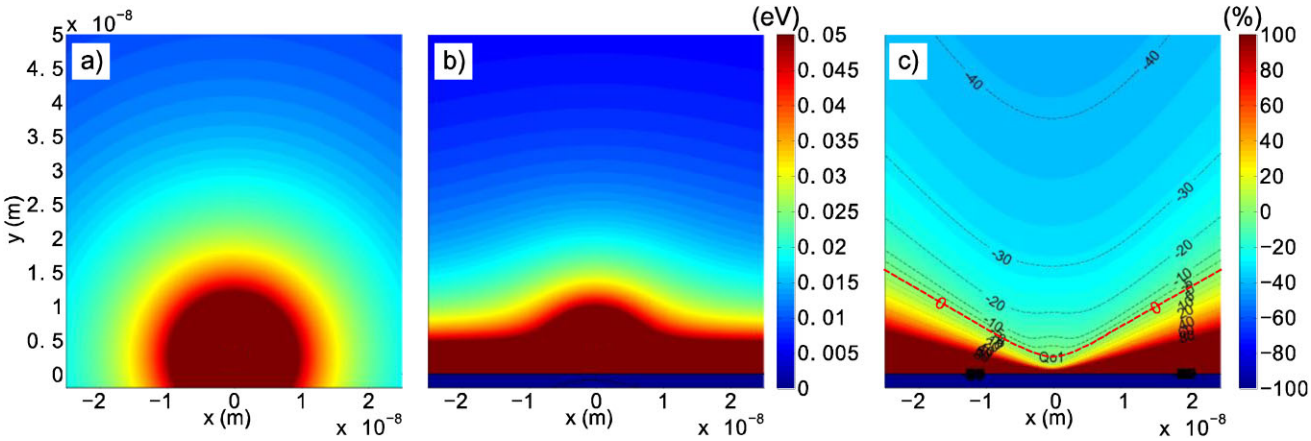


**Figure 2** (a) Escape energy for $Q_t$ at a low-$k$/low-$k$ ($\varepsilon_{r,\text{low-}k} = 3/\varepsilon_{r,\text{low-}k} = 3$) interface, (b) escape energy for $Q_t$ at a low-$k$/high-$k$ ($\varepsilon_{r,\text{low-}k} = 3/\varepsilon_{r,\text{high-}k} = 300$) interface, (c) relative change in the escape energy between the cases (a) and (b).

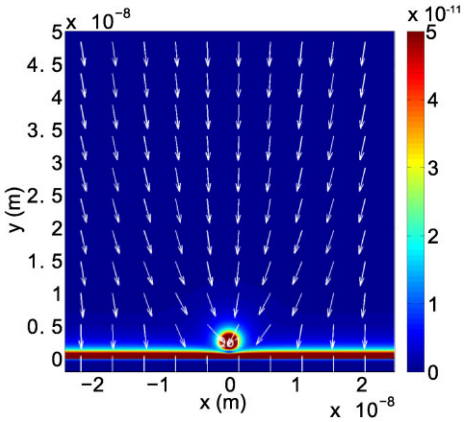


**Figure 3** Force affecting $Q_t$ at a low-$k$/high-$k$ interface ($\varepsilon_{r,low\text{-}k} = 3/\varepsilon_{r,high\text{-}k} = 300$). White arrows indicate the direction of the force.

strongly screened at the cost of a strong charge interaction with the interface itself. However, if charge carrier transport parallel to the high-$k$ interface is possible, using device concepts as introduced in the following, the interface interaction will not limit electronic transport through the device and therefore not limit the benefit of the effectively enhanced organic semiconductor permittivity for organic photovoltaic applications.

The benefit of the introduced concept can be summarized by a reduction of the electrostatic charge carrier interaction in organic semiconductors. This has the following consequences: (1) a reduction of the exciton binding energy [14] and (2) a reduction of the non-geminate recombination probability due to screened complementary charges during charge carrier transport. Aspect 2 is especially important for organic bulk heterojunction solar cells, where after efficient exciton separation and because of long reaching Coulomb interaction, the parallel complementary charge transport in the respective acceptor–donor phases will lead to charge pair formation and in consequence to recombination losses.

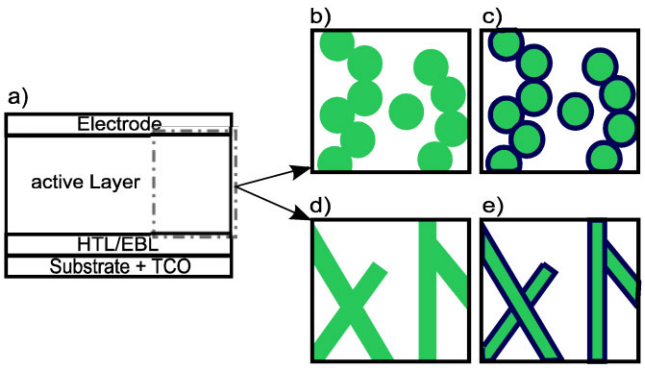


**Figure 4** Organic bulk-heterojunction photovoltaic cell (a) typical device structure, (b) with integrated high-$k$ percolating nanoparticles; (c) case (b) modified with an organic coating; (d) with integrated nanowires and (e) case (d) modified with organic coating.

**4 Device concepts and first devices** In order to make use of the introduced concept for organic solar cell applications, structures as shown in Fig. 4 are suggested. Here, the active layer is made up of a hybrid structure consisting of an organic acceptor/donator system with integrated inorganic electrically insulating, nanostructured high-$k$ materials.

Amongst other implementation possibilities the concept can be realized by the integration of either high-$k$ nanoparticles or nanowires. As long as percolation along the particles or nanowires between the respective electrodes of the organic solar cell is possible, the structure should not be limited by the discussed charge carrier/high-$k$ interface interaction. To insure a good dispersability of the nanostructures in an organic solvent alongside the acceptor/donor material and to positively influence the thin film morphology, a functionalization might become necessary. However, due to the demonstrated long reaching influence of the charge carrier screening, a functionalization should not limit the concept. The structures as described so far may, however, result in recombination losses as illustrated in Fig. 5, where the high-$k$ nanostructure interconnects acceptor and donor phases and in consequence may lead to the trapping of complementary charges. Encasing the nanostructures with either an organic acceptor or donor material prior to dispersion, as suggested by Fig. 4c and e may therefore further improve the discussed approach.

To test the feasibility of the discussed concept for an organic photovoltaic application, first P3HT:PCBM devices containing high-$k$ $SrTiO_3$ nanoparticles were implemented according to approach A, as described in the experimental section. The nanoparticle distribution in the organic active layer is illustrated by the thin film top view scanning electron microscopy (SEM) image shown in Fig. 6. The nanoparticles form agglomerates which are evenly distributed over the whole sample area. This structure is well described by the concept depicted in Fig. 4b, as demonstrated by the inset of Fig. 6. It substantiates nanoparticle agglomerates forming percolation paths through the active layer. The anode–cathode percolation path ensures (a) charge carrier transport through the device parallel to the high-$k$ interface as discussed above, and (b) unproblematic charge carrier extraction at the electrodes, as the permittivity of the

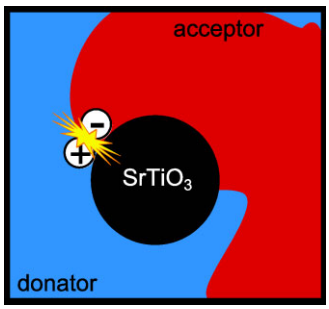


**Figure 5** Limit to the concept by recombination when high-$k$ nanostructures interconnect acceptor/donor phases.

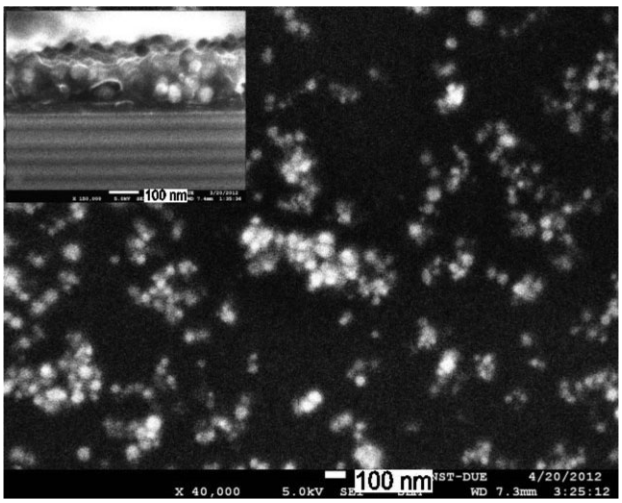


**Figure 6** SEM image of the P3HT:PCBM thin film with integrated $SrTiO_3$ nanoparticles and inlay cross-section of the same.

electrodes exceeds the permittivity of the $SrTiO_3$. Further thin film morphology improvements are ongoing research.

Illustrated in Fig. 7a is the *I–V* characteristic of a P3HT:PCBM:$SrTiO_3$ device in comparison to a P3HT:PCBM reference. The devices were measured in the dark as well as under AM1.5 standard illumination. In comparison to the reference device, the short circuit current for the high-*k* cell has been reduced by ~3.6% from $J_{sc} = 7.9\,mA\,cm^{-2}$ down to $J_{sc} \sim 7\,mA\,cm^{-2}$. The fill factors (FF) on the other hand, as well as the open circuit voltages ($V_{oc}$) have been improved by ~10%. The FF shows an improvement from 0.49 (reference) up to 0.54 (high-*k*), while the open circuit voltage has been increased from $V_{oc} = 0.52\,V$ (reference) up to $V_{oc} = 0.57\,V$ (high-*k*). In terms of power conversion efficiency, this translates into an efficiency improvement for the high-*k* solar cell of ~17% from $\eta = 2\%$ absolute for the reference cell up to $\eta = 2.34\%$ absolute for the high-*k* cell. Statistical data confirming the discussed performance enhancement for high-*k* organic devices is illustrated in Table 1. Here, average values of two P3HT:PCBM reference devices are compared with the average values of seven SrTiO3:P3HT:PCBM devices. Further the two sigma standard deviation is specified for the SrTiO3:P3HT:PCBM cells. A relatively high standard deviation is found for the $\eta$ and $J_{sc}$ values, which are each the consequence of a higher deviation for one out of the seven high-*k* cells. These outlier cells are suggested to be the result of non-optimized processing conditions.

It should be noted that the obtained absolute efficiencies of ~2% for both reference and high-*k* devices are lower than one would expect for a standard P3HT:PCBM system, where efficiencies in the order of ~3.5% are a good average [16, 17]. This deviation is ascribed to the extensive stirring times of ~24 h at $T = 65$–$70\,^{\circ}C$ during the preparation of the P3HT:PCBM solution. The extensive stirring time was required to disperse the $SrTiO_3$ nanoparticles and as such may lead to a degradation of the organic semiconductor or morphology effects which possibly degrade the short circuit current. However, since both the reference cells as well as the high-*k* cells were realized with solutions/dispersions exposed to identical stirring times, this preliminary experimental circumstance still allows for an interpretation of the influence of the high-*k* nanoparticles on the organic solar cell performance.

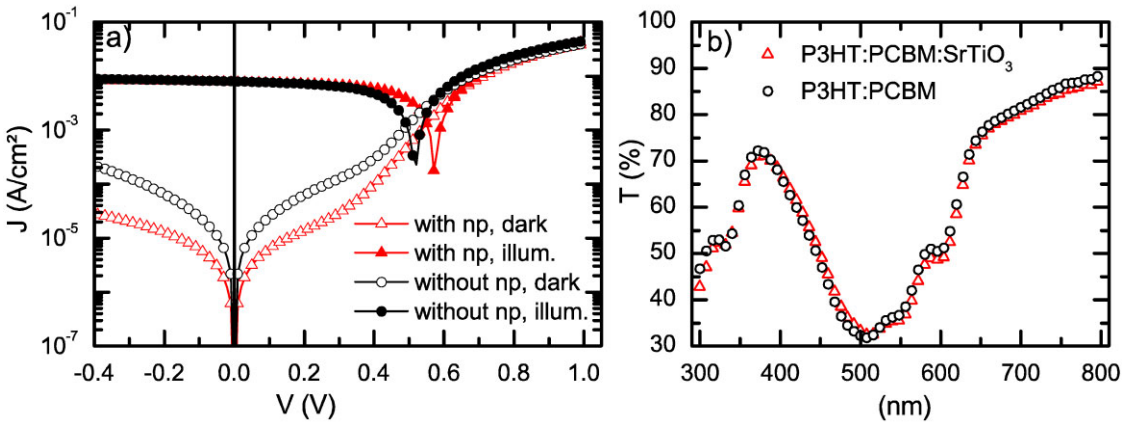


**Figure 7** (a) *I*(*V*)-characteristics of a P3HT:PCBM:$SrTiO_3$ solar cell and of a P3HT:PCBM reference device, (b) transmission spectrum of P3HT:PCBM:$SrTiO_3$ and P3HT:PCBM thin films.

**Table 1** Average solar cell parameters and $2\sigma$ standard deviations.

| | $\eta_{ave}$ (%) | $2\sigma$ | $V_{oc,\,avg}$ (V) | $2\sigma$ | $J_{sc,\,avg}$ (mA cm$^{-2}$) | $2\sigma$ | FF | $2\sigma$ |
|---|---|---|---|---|---|---|---|---|
| P3HT:PCBM (2 cells) | 2.07 | – | 0.54 | – | 8.11 | – | 0.48 | – |
| SrTiO3:P3HT:PCBM (7 cells) | 2.25 | 0.46 | 0.57 | 0.016 | 7.73 | 0.86 | 0.51 | 0.0654 |

By considering Fig. 7b, which illustrates the result of a transmission measurement experiment on P3HT:PCBM thin films with and without $SrTiO_3$ nanoparticles, we find that the thin film transmission does not change due to the nanoparticle integration. Conducted reflection measurements (not shown) yield the same result. This allows us to conclude that the obtained power conversion efficiency improvement for the organic solar cell with integrated nanoparticles is not the result of light-scattering effects and as such an enhanced optical path length within the cell. Further, by observing that $J_{sc}$ is reduced and $V_{oc}$ is enhanced upon nanoparticle integration, we can exclude beneficial morphology effects as a cause for the enhanced efficiency. We conclude the enhanced power conversion efficiency of the solar cells with integrated $SrTiO_3$ particles to be the result of an effectively enhanced device permittivity. The development of $J_{sc}$ and $V_{oc}$ upon nanoparticle integration supports this statement. For P3HT:PCBM organic solar cells, with an exciton separation efficiency close to 100%, at the acceptor/donor heterointerface, no significant further improvement of the exciton separation efficiency is to be expected, and therefore no improvement in the short circuit current [16, 18]. However, due to the enhancement of the effective system permittivity, we anticipate a reduction of the non-geminate recombination probability during charge carrier transport in the bulk heterojunction system as the result of reduced Coulomb interaction. This can be described by an enhanced macroscopic shunt resistance, as shown by the equivalent circuit in Fig. 8, and has the following consequence for $J_{sc}$ and $V_{oc}$. In principle an increased shunt resistance may lead to an enhancement of the $J_{sc}$ value, simply because of the characteristic of the $R_{sh}/R_s$ current divider. For the experiment however, a decrease in $J_{sc}$, is observed. This may be a consequence of the integrated $SrTiO_3$ nanoparticles and the resulting reduction in the photoactive fraction of the organic thin film. However, since the nanoparticle integration does not influence the transmission or reflection properties of the P3HT:PCBM thin film, as discussed for Fig. 7b, we suggest the reduction in $J_{sc}$ to be the result of a non optimized semiconductor morphology upon nanoparticle integration. An enhanced macroscopic $R_s$ value for the discussed high-$k$ organic solar cells would be the consequence, canceling out the improvement in $J_{sc}$ anticipated for an enhanced $R_{sh}$ value.

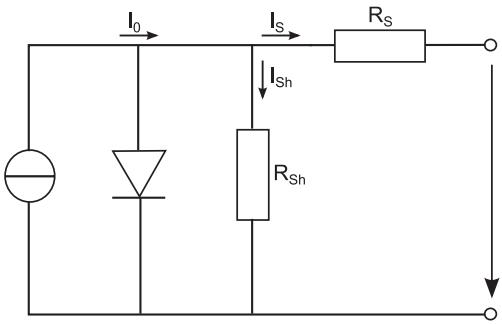


**Figure 8** Simplified equivalent circuit diagram, where the current source stands for the exciton dissociation and decrease of the shunt resistance is a consequence of bimolecular recombination.

Independent of a potential reduction in photoactive medium due to high-$k$ nanoparticle integration, or a possible changed series resistance value due to morphology influences, however, is the impact of the enhanced $R_{sh}$ on $V_{oc}$, as can be derived using the equivalent circuit in Fig. 8. An enhancement in $V_{oc}$ is expected for an enhanced $R_{sh}$ and as such a reduced non-geminate recombination probability. This conclusion is supported by the determined low standard deviation observed for $V_{oc}$ as illustrated in Table 1.

We have indicated above that the introduced concept has no influence on the exciton separation efficiency at the acceptor/donor interface. While this may be true for P3HT:PCBM, with its inherent large energetic transport state offset at the heterointerface, the concept does have the potential to allow for a reduced energetic offset at the heterojunction, *e.g.*, by the use of different semiconductor combinations and still allow for efficient exciton separation. This is suggested since a reduced coulomb interaction will certainly reduce the exciton binding energy, as recently demonstrated for pentacene on substrates with different permittivities [14].

**5 Conclusions** In conclusion we introduced a new concept to enhance the effective permittivity of organic semiconductor thin films, by the integration of electrically insulating, nanostructured high-$k$ materials. This concept is intended for an application in organic photovoltaic cells. Using an analytical model we substantiated that an enhancement of the effective organic thin film permittivity will reduce the Coulomb interaction in the organic layer, and as such will improve charge carrier transport properties. This was experimentally verified by realizing first P3HT:PCBM:$SrTiO_3$ nanoparticle test devices, which demonstrate an enhanced power conversion efficiency of ~17% in comparison to a P3HT:PCBM reference device. This improvement is ascribed to a reduction in non-geminate recombination, which is in line with the influence of an effectively enhanced organic layer permittivity.

**Acknowledgements** The authors acknowledge funding within the framework of a North Rhine-Westphalia scholarship for "rollable solar cells". Further, the group of Prof. G. Bacher, located at the University of Duisburg-Essen, is acknowledged for making the transmission and reflection measurements possible.

## References

[1] M. A. Green, K. Emery, Y. Hishikawa, W. Warta, and E. D. Dunlop, Prog. Photovolt.: Res. Appl. **20**, 12 (2012).
[2] Heliatek, press release, 10.7% organic tandem solar cell (April, 2012).
[3] C. Deibel and V. Dyakonov, Rep. Prog. Phys. **73**, 096401 (2010).
[4] G. Yu, J. Gao, J. C. Hummelen, F. Wudl, and A. J. Heeger, Science **270**, 1789 (1995).

[5] J. Meiss, T. Menke, K. Leo, C. Uhrich, W.-M. Gnehr, S. Sonntag, M. Pfeiffer, and M. Riede, Appl. Phys. Lett. **99**, 043301 (2011).
[6] B. V. Andersson, N.-K. Persson, and O. Inganas, J. Appl. Phys. **104**, 124508 (2008).
[7] M. Pope and C. E. Swenberg, Electronic Processes in Organic Crystals and Polymers (Oxford University Press, New York, USA, 1999).
[8] S. E. Gledhill, B. Scott, and B. A. Gregg, J. Mater. Res. **20**, 3167 (2005).
[9] M. Knupfer, Appl. Phys. A **77**, 623 (2003).
[10] R. A. Marsh, J. M. Hodgkiss, and R. H. Friend, Adv. Mater. **22**, 3672 (2012).
[11] C. Deibel, T. Strobel, and V. Dyakonov, Phys. Rev. Lett. **103**, 036402 (2009).
[12] L. J. A. Koster, S. E. Shaheen, and J. C. Hummelen, Adv. Energy Mater. **2**, 1246 (2012).
[13] M. Lenes, F. B. Kooistra, J. C. Hummelen, I. Van Severen, L. Lutsen, D. Vanderzande, T. J. Cleij, and P. W. M. Blom, J. Appl. Phys. **104**, 114517 (2008).
[14] M. Engel, F. Kunze, D. C. Lupascu, N. Benson, and R. Schmechel, Phys. Status Solidi RRL **6**, 68 (2012).
[15] J. D. Jackson, Classical Electrodynamics (John Wiley & Sons, New York, 1998).
[16] M. Mingebach, S. Walter, V. Dyakonov, and C. Deibel, Appl. Phys. Lett. **100**, 193302 (2012).
[17] P. A. Troshin, H. Hoppe, A. S. Peregudov, M. Egginger, S. Shokhovets, G. Gobsch, N. S. Sariciftci, and V. F. Razumov, ChemSusChem **4**, 119 (2011).
[18] J. Guo, H. Ohkita, H. Benten, and S. Ito, J. Am. Chem. Soc. **132**, 6154 (2010).

 